Analysis of the Subsurface Volume of Differently Finished AISI 52100 by Cyclic Indentation and X-Ray Diffraction

Pascal Ostermayer, Werner Ankener, Bastian Blinn, Marek Smaga, Dietmar Eifler, and Tilmann Beck*

Dedicated to Prof. Dr.-Ing. Wolfgang Bleck on the occasion of his 70th birthday

Finishing processes result in changes of near-surface morphology, which strongly influences the fatigue behavior of components. Especially, roller bearings show a high dependency of the lifetime on surface roughness and the residual stress state in the subsurface volume. To analyze the influence of different finishing processes on the near-surface morphology, including the residual stress state, roller bearing rings made of AISI 52100 are finished in this work using hard turning, rough grinding, and fine grinding. In addition, fatigue specimens made of AISI 52100 and finished by cryogenic hard turning are investigated. For each condition, the residual stresses are determined at different distances from the surface, showing pronounced compressive stresses for all conditions. While the ground roller bearing rings show highest compressive residual stresses at the surface, the hard turned bearing ring and the cryogenic hard turned fatigue specimens reveal maximum compressive stresses in the subsurface volume. Moreover, cyclic indentation tests (CITs) are conducted in the different subsurface volumes, showing a higher cyclic plasticity in relation to the respective initial state, which is assumed to be caused by finishing-induced compressive residual stresses. Thus, the presented results indicate a high potential of CITs to efficiently characterize the residual stress state.

1. Introduction

The surface as well as the near-surface morphology of nearly any material play an important role for the application of a component and significantly impacts its lifetime, which is determined by wear[1,2] and fatigue.[3–5] While the surface is mostly represented by the topography, which directly influences the wear resistance, the subsurface morphology comprises the whole complexity of the existing microstructure, its residual stress state, and the resulting mechanical properties. In this context, especially the residual stresses within the subsurface volume are important for the endurance of cyclically loaded components, for example, roller bearings. As discussed, for roller bearing rings, the highest load-induced stresses are located below the surface[6,7] due to the Hertzian contact to the roller elements. Consequently, not only the surface topography, which affects the lubrication and the wear behavior,[8,9] but also the subsurface morphology have to be improved to increase the fatigue life of roller bearing rings.

In industry, roller bearing rings are commonly made of AISI 52100 bearing steel using hard turning as well as grinding processes. Furthermore, innovative cryogenic hard turning processes are currently explored to produce a well-defined, beneficial surface and subsurface morphology of AISI 52100.[10–14] Depending on the manufacturing parameters, all these finishing processes, that is, conventional hard turning, cryogenic hard turning, and grinding, can be used to introduce compressive residual stresses in the subsurface volume,[15,16] which lead to a significantly enhanced fatigue life of roller bearing rings.[6,7,17,18] The influence of the residual stresses in the subsurface volume on the fatigue behavior of roller bearing rings is very well described in literature[6,7,17,18] and has been used to model the service lifetime of roller bearings.[7,17,19] This underlines the importance of the residual stress state within the subsurface volume for the application of roller bearing rings. However, in addition to the residual stress state, the local microstructure and the resulting mechanical properties of the subsurface volume have to be considered for a thorough analysis of the fatigue behavior, which further enables an adjustment of the subsurface volume by finishing.

To locally analyze the mechanical properties of a material, indentation testing can be used, whereby smaller indentation forces lead to a higher spatial resolution.[20,21] In addition to conventional indentation testing, instrumented cyclic indentation tests (CITs), which are the basis of the short-time method PhyBaL$_{CHT}$,[22] can be used to determine the cyclic deformation behavior of a material.[23–25] By decreasing the indentation force, this testing approach was successfully used to characterize the

P. Ostermayer, W. Ankener, B. Blinn, M. Smaga, D. Eifler, T. Beck
Institute of Materials Science and Engineering
TU Kaiserslautern
67663 Kaiserslautern, Germany
E-mail: beck@mv.uni-kl.de

The ORCID identification number(s) for the author(s) of this article can be found under https://doi.org/10.1002/srin.202100253.

cyclic properties of the subsurface volume of a high-Mn twinning induced plasticiocity (TWIP) steel HSD600,[26] as well as in the vicinity of a fatigue crack of a fully ferritic high-Cr steel.[27] Moreover, the indentation force F and indentation depth h hysteresis loops obtained in CITs have been modeled at atomistic scale using molecular dynamic simulation.[28] Furthermore, the analysis of the cyclic deformation behavior obtained in CITs can be used to determine the cyclic hardening potential of a material. As shown in different types of conventionally manufactured steels,[22,23,29] as well as additively manufactured AISI 316L,[30] the cyclic hardening potential determined by means of PhyBaL$_{CHT}$ correlates very well with the defect tolerance of a material.

In the present work, CITs and X-ray diffraction (XRD) were used to characterize the subsurface volume of differently manufactured AISI 52100-bearing steel. Therefore, roller bearing rings were industrially manufactured using hard turning, rough grinding, and fine grinding. In addition to these commonly used finishing processes, fatigue specimens were cryogenically hard turned, which represents an innovative machining process of great scientific interest. By conducting CITs, an analysis of the local cyclic deformation behavior can be obtained, which is complemented by the respective residual stress state. This combination of CITs and measurement of residual stresses enables a thorough analysis of the mechanical properties of the finishing-induced subsurface volumes.

2. Experimental Section

2.1. Investigated Materials and Specimens

To investigate the influence of the finishing processes on the resulting morphology of the subsurface volume, which comprises, in the present work, the surface and the volume beneath the surface up to a distance from the surface of $\approx 50-60\,\mu m$, two batches of the roller bearing steel AISI 52100 with slightly different chemical compositions (see **Table 1**) were differently finished. Therefore, established finishing processes as well as innovative cryogenic hard turning were conducted. While batch A was used for manufacturing roller bearing rings, cylindrical fatigue specimens were turned from batch B (see **Figure 1**).

The manufacturing of the roller bearing rings was conducted by Interprecise Donath GmbH (Obermichelbach, Germany) using three different finishing processes, that is, hard turning, rough grinding, and fine grinding. In addition to the finishing processes established in industrial application, the fatigue specimens made from batch B were cryogenic hard turned, which represents an innovative finishing process, being of high scientific interest.[14,31] For the fatigue specimens, two sets of manufacturing parameters were used to induce significantly different morphologies of the subsurface volume. Cryogenic turning was conducted by the Institute for Manufacturing Technology and

Production Systems of TU Kaiserslautern. The parameter sets used are given as follows.

1) Parameter set 1 (P1): feed $f = 0.15\,mm\,rev^{-1}$, cutting speed $v_C = 150\,m\,min^{-1}$, cutting depth $a_p = 0.05\,mm$, mass flow $\dot{m}_{CO_2}$ $\dot{m}_{CO_2} = 0.75\,kg\,min^{-1}$, width of wear marks VB = 0 μm, and cutting edge radius $r_\beta = 10\,\mu m$.

2) Parameter set 2 (P2): $f = 0.10\,mm\,rev^{-1}$, $v_C = 50\,m\,min^{-1}$, $a_p = 0.05\,mm$, $\dot{m}_{CO_2} = 1.50\,kg\,min^{-1}$, VB = 100 μm, $r_\beta = 80\,\mu m$.

Both batches were austenitized in a controlled carbonaceous atmosphere to prevent decarburization and were subsequently quenched and tempered, before machining and subsequently finishing to the final geometry. Note that the conditions of the heat treatments, which are shown in detail in **Table 2**, significantly differ between batch A and batch B.

These heat treatments resulted for both batches in a consistent martensitic microstructure, showing finely dispersed chromium carbides, which were less pronounced for the fatigue specimens of batch B, presumably caused by the lower tempering temperature (see **Figure 2**). However, for both batches, the finishing process did not lead to significant changes in the microstructure within the subsurface volume, which was nearly identical to the core material. This is exemplarily shown in Figure 2 for the hard turned roller bearing ring (batch A) and the fatigue specimen cryogenic hard turned with parameter set P2 (batch B). To obtain a detailed visualization of the microstructure within the subsurface volumes and core materials, the cross sections were etched with a Nital etchant.

Note that batch A and batch B differ in the material condition, specimen geometry, as well as finishing processes used, which disables a direct comparison. Consequently, the influence of the finishing processes on the subsurface volume has to be analyzed separately for each batch.

To conduct the instrumented CITs at the roller bearing rings, cross sections of the whole components were extracted from the middle, whereas the CITs at the fatigue specimens were conducted on cross sections of the gauge length (see Figure 1). This led to indentation directions parallel to the axial direction of both, the roller bearing rings and the fatigue specimens (see **Figure 3**). To extract the cross sections, cutting with a low feed rate and a high mass flow of the cooling lubricant was used to avoid changes in the microstructure. Finally, the cross sections were mechanically polished to achieve a mirror flat surface, being necessary for microindentation testing. For polishing, small forces were applied to not introduce residual stresses during the preparation process.

With XRD, the manufacturing-induced residual stresses within the subsurface volume were analyzed. The XRD measurements were carried out on the peripheral surface of the fatigue specimens and roller bearing rings, as shown in Figure 1. To obtain a depth-resolved characterization of the residual stresses, the surfaces of the fatigue specimens and the roller bearing rings were iteratively removed by electrolytic polishing with Struers LectroPol-5, whereby

Table 1. Chemical composition of the AISI 52 100 batches.

Amount of alloying element [wt.−%]	C	Si	Mn	P	S	Cr	Ni	Al	N	Mo
Batch A: Roller bearing rings	0.98	0.24	0.37	0.009	0.014	1.46	0.13	0.014	0.014	0.030
Batch B: Cryogenic hard turned fatigue specimens	0.94	0.32	0.37	0.005	0.003	1.43	0.02	0.001	0.007	0.002

**ADVANCED
SCIENCE NEWS**

www.advancedsciencenews.com

**steel
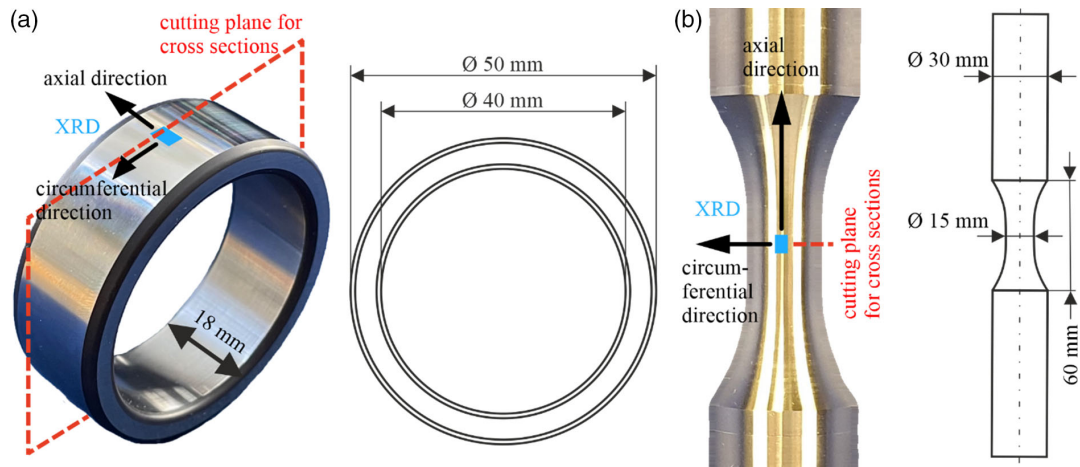research**
international

www.steel-research.de

Figure 1. Illustration of the components investigated: a) roller bearing ring and b) fatigue specimen, including geometrical dimensions, directions, and positions of the residual stress measurements by means of XRD.

Table 2. Heat treatment parameters used for the different batches of AISI 52100 as well as resulting macrohardness.
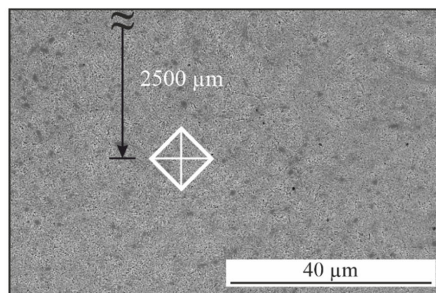
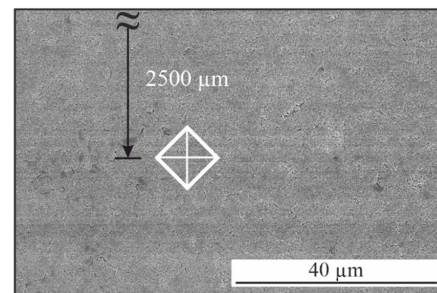|	Austenitization	Quenching	Tempering	Hardness
Batch A: Roller bearing rings	850 °C/45 min	180 °C/15 min	240 °C/240 min	730 ± 7 HV30
Batch B: Cryogenic hard turned fatigue specimens	850 °C/120 min	Oil temperature < 80 °C	180 °C/10^4 min	783 ± 7 HV30
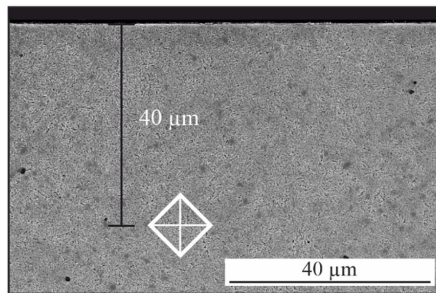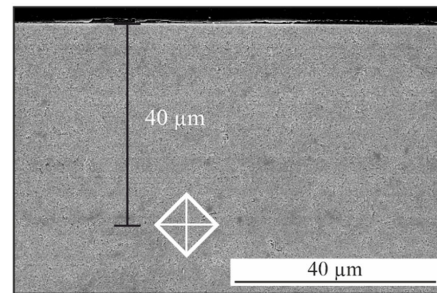
Figure 2. Microstructure of the subsurface volume and core material of a,c) hard turned roller bearing ring and b,d) cryogenic hard turned fatigue specimen, including the typical size of the indent resulting from CITs.

XRD measurements were carried out after each polishing step. To avoid microstructural changes during the polishing process, the electrolyte was permanently cooled to temperatures between 0 and 20 °C. Note that the changes in residual stress state caused by electrolytic polishing can be neglected, as in relation to the geometries of the bearing rings and the fatigue specimens
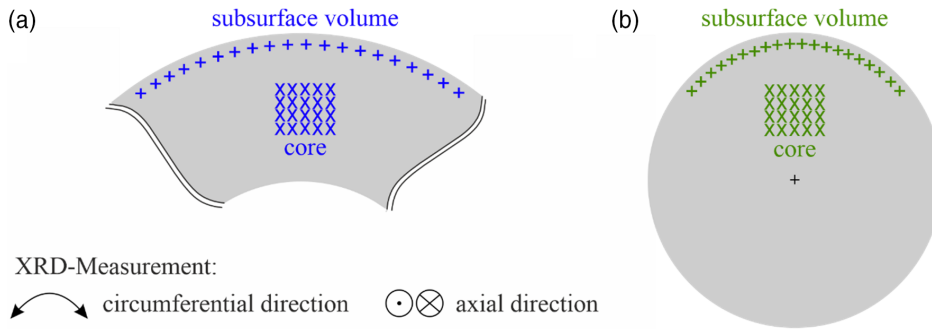
**ADVANCED
SCIENCE NEWS**

www.advancedsciencenews.com

**steel
research**
international

www.steel-research.de

Figure 3. Schematic description of the positioning of the indentation points on the cross sections of a) the roller bearing rings and b) the cryogenic hard turned fatigue specimens.

only small areas $(20\,\text{mm} \times 10\,\text{mm})$[32] as well as depths $(100-150\,\mu\text{m})$[33] were removed. Thus, no mathematical compensation of the residual stresses is required for the presented results.

2.2. Cyclic Indentation Tests

To analyze the influence of the different finishing processes on the local mechanical, and especially cyclic properties within the subsurface volume, the short-time method PhyBaL$_{CHT}$ was used, which is explained in detail in previously published works.[22,23] Therefore, instrumented CITs were conducted with Fischerscopes of types H100C and HM2000 (Helmut Fischer GmbH, Germany), which enabled a continuous detection of the indentation depth h and the indentation force F. The indentations were conducted on the cross sections of the different types of specimens, as shown schematically in Figure 3. During the CITs, the material was loaded for ten cycles with a sinusoidal load function by a Vickers indenter, whereby a maximum indentation force $F_{\text{max}} = 500\,\text{mN}$ and a frequency of 1/12 Hz were applied. From the second cycle on, an $F-h$ hysteresis can be obtained in CITs, which is schematically shown in **Figure 4**a. In analogy to the plastic strain amplitude $\varepsilon_{\text{a,p}}$ obtained from stress−strain hysteresis, the half width of the $F-h$ hysteresis at mean loading $(0.5\,F_{\text{max}})$ is defined as the plastic indentation depth amplitude $h_{\text{a,p}}$, which can be used as a characteristic value of plastic deformation during the respective indentation cycle. By analyzing the change in $h_{\text{a,p}}$ during the CITs, which is represented by $h_{\text{a,p}}-N$ curve, the cyclic deformation behavior of the material can be analyzed (see Figure 4b). From the fifth cycle on, the $h_{\text{a,p}}-N$ curve reveals a stabilized slope, indicating a saturation of macroplastic deformation and that microplasticity subsequently dominates the cyclic deformation behavior. Moreover, this regime can be described mathematically by the power law function $h_{\text{a,p II}}$ (Equation (1)), whereby the cyclic hardening exponent$_{CHT}$ e_{II} represents the slope of the $h_{\text{a,p}}-N$ curve in this regime (see Figure 4b). As a steeper slope of $h_{\text{a,p}}-N$ curve results from more pronounced cyclic hardening, higher $|e_{II}|$ correlates with a greater cyclic hardening potential of the material.[22]

$$h_{\text{a,p II}} = a_{II} \cdot N^{e_{II}} \tag{1}$$

Besides the analysis of cyclic hardening, the $h_{\text{a,p}}-N$ curve can be used to describe the cyclic plasticity of the material. As higher $h_{\text{a,p}}$ is caused by more pronounced plastic deformation, the vertical
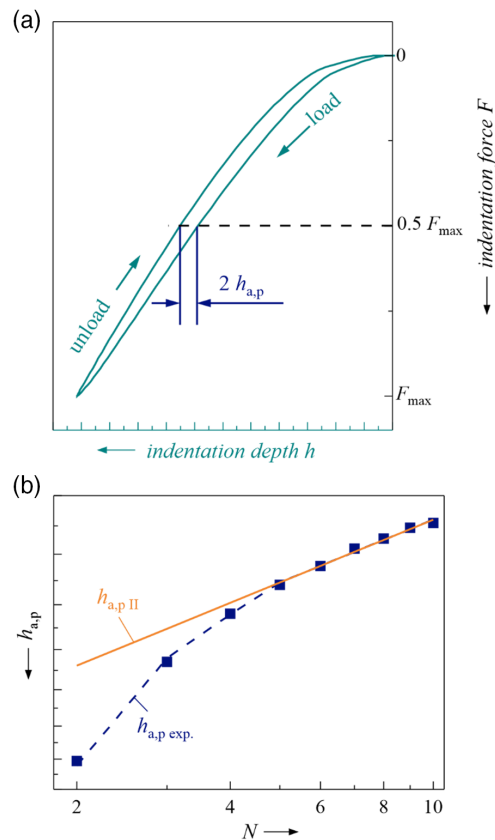

Figure 4. Schematic description of a) the $F-h$ hysteresis and b) the $h_{\text{a,p}}-N$ curve obtained in CITs according to the study by Kramer et al.[22]

position of the $h_{\text{a,p}}-N$ curve can be related to cyclic plasticity. By comparing the position of the $h_{\text{a,p}}-N$ curves of different material conditions, the amount of cyclic hardening and thus, cyclic hardening exponent$_{CHT}$ e_{II}, as well as the absolute value of the indentation depth h, have to be considered. However, if different conditions show comparable absolute indentation depths and $|e_{II}|$, the $h_{\text{a,p}}-N$ curves can be used for a sufficient assessment of cyclic plasticity.

In addition to the analysis of the cyclic properties, the indentation depth resulting from the first cycle can be used to determine the microhardness (Marten's hardness, HM) of the material.

To analyze the differences in the microhardness and the cyclic deformation behavior between the subsurface volume, being modified by the finishing process, and the unaffected core, representing the initial state of the material, the CITs were conducted for each specimen in a distance from the edge of 40 μm as well as 2.5 mm (see Figure 2). For both positions, a minimum of 20 CITs were conducted to obtain statistically reliable results. Note that the plastically deformed volume beneath the indenter can roughly be estimated with a factor 3 of the indent diagonal.[20] Because the indent diagonals in this work were ≈12 μm, a minimum distance from the surface of 40 μm was chosen in accordance with DIN EN ISO 14577.[34] Moreover, the different indentation points were placed with a point-to-point distance of at least 100 μm to exclude interference effects.

2.3. Scanning Electron Microscopy

The microstructural images shown in Figure 2 were taken using an secondary electrons (SE) detector in a scanning electron microscope (SEM) of the type FEI Quanta 600. For these investigations, an acceleration voltage of 20 kV and a working distance of 10 mm were used.

2.4. X-Ray Diffraction

The analyses of the residual stresses were conducted with two types of X-ray diffractometers, that is, of the type PANalytical X'Pert PRO MRD to investigate the roller bearing rings, as well as PANanlytical Empyrean to characterize the fatigue specimens. For both systems, Cu Kα$_1$ radiation at 40 kV tube voltage and 40 mA tube current as well as a scanning speed of 0.004°/s were used. While the size of the irradiated spot was 3 mm × 2 mm for the measurements of the roller bearing rings, a spot size of 3.7 mm × 2.4 mm was used for the analysis of the fatigue specimens (see Figure 1). For both types of specimens, that is, bearing rings and fatigue specimens, the first-order residual stresses were measured for all depths in axial and circumferential direction with the sin²ψ method applied to the diffraction peak of the {211} martensite lattice plane. The sin²ψ method offers the advantage that the plane spacing is determined by considering several tilt angles ψ, which are defined as the angle between the beam path and the normal of the specimen surface.

This enables a high accuracy of the determined residual stress state.[35]

3. Results

3.1. Influence of the Finishing Process on the Mechanical Properties and Cyclic Deformation Behavior of the Subsurface Volume

3.1.1. Batch A: roller bearing Rings

Comparing the microhardness of the differently finished roller bearing rings, no significant difference appears between the subsurface volume, and the core material, respectively (see **Figure 5**a). Note that the indentations in the subsurface volume were conducted at a distance from the surface of 40 μm and hence, only provide information of the material volume within the sector between the surface distances of roughly 25 and 55 μm. For smaller indentation forces and thus, higher spatial resolution, a higher hardness in the vicinity of the outer surface is assumed, which, however, was not objective of the present work. For the different finishing processes, that is, hard turning, rough grinding, and fine grinding, comparable hardness values were determined.

The results obtained for microhardness correlate well with the values of cyclic hardening exponent$_{CHT}$ e_{II}, which also show no significant difference between the different finishing conditions as well as between the subsurface volumes and the core materials (see Figure 5a). Consequently, HM and e_{II} indicate no substantial influence of the finishing process on the mechanical properties of the subsurface volume, which correlates well with the microstructural analyses, showing no process-induced microstructural changes (see Figure 2a,c).

As HM and e_{II} are nearly identical between the different conditions as well as the subsurface volumes and the core materials, the cyclic plasticity can be evaluated by comparing the vertical positions of the $h_{a,p}-N$ curves. In **Figure 6**, the $h_{a,p}-N$ curves obtained from the subsurface volume and the core material are compared for the different finishing processes. Note that the vertical axis of $h_{a,p}-N$ curves is shown in reverse direction in Figure 6. For all conditions, a higher cyclic plasticity is observed within the subsurface volume, which is more pronounced for the hard turned and fine ground roller bearing rings. Thus, in contrast to HM, e_{II}, and the microstructural
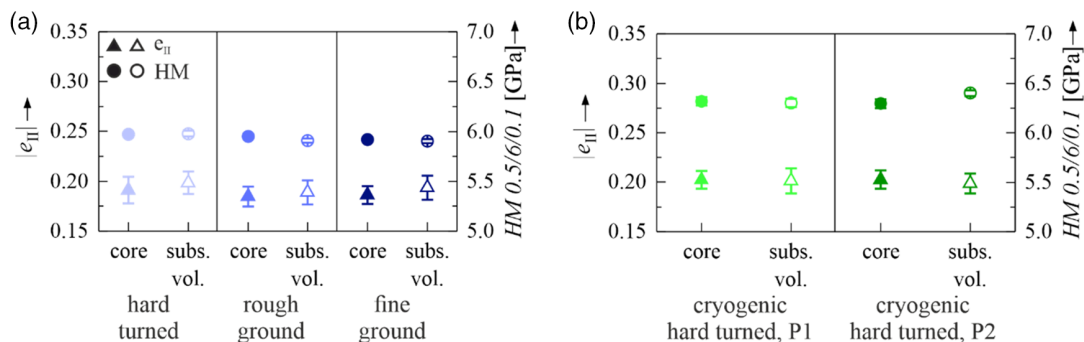
Figure 5. Cyclic hardening exponent$_{CHT}$ e_{II} and microhardness HM obtained in CITs at a) differently finished roller bearing rings and b) cryogenic hard turned fatigue specimens.

**ADVANCED
SCIENCE NEWS**

www.advancedsciencenews.com

**steel
research**
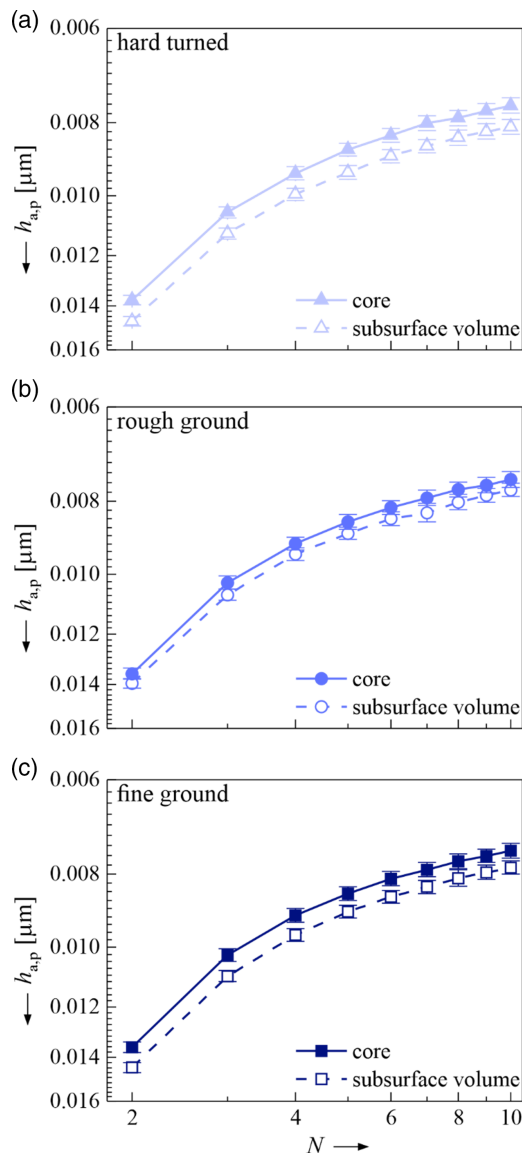international

www.steel-research.de

Figure 6. Comparison of the $h_{a,p}-N$ curves obtained in CITs within the subsurface volume and the core material of a) hard turned, b) rough ground, and c) fine ground roller bearing rings.

investigations, the $h_{a,p}-N$ curves reveal changes in the mechanical properties of the subsurface volumes, which were induced by the finishing processes used.

3.1.2. Batch B: Fatigue Specimens

Similar to the results of the roller bearing rings (batch A), the microhardness HM as well as the cyclic hardening exponent$_{CHT}$ e_{II} show for both conditions of cryogenic hard turned specimens no clear difference between the subsurface volume and the core material, which correlates with the microstructural SEM observations (compare Figure 5b with 2b,d). The different parameter sets P1 and P2 result in comparable

microhardness as well as cyclic hardening potential, which also correlates with the results obtained from roller bearing rings.

Comparing the different batches, the fatigue specimens of batch B show higher hardness than the roller bearing rings of batch A, which is caused by the lower tempering temperature (see Figure 5 and Table 2). Despite the different hardness and tempering temperature, the cyclic hardening potential, represented by e_{II}, is comparable for the different batches.

Similar to the investigations of the roller bearing rings, the $h_{a,p}-N$ curves obtained from cryogenic hard turned fatigue specimens can be used to analyze the changes in cyclic plasticity. As shown in **Figure 7**, for both conditions, the subsurface volume reveals a slightly higher cyclic plasticity than the core material. Comparing P1 and P2, the increase in cyclic plasticity is slightly more pronounced after cryogenic turning with parameter set P2. The increase in cyclic plasticity of the subsurface in relation to the core volume corresponds to the results of batch A. However, this effect is significantly less pronounced for cryogenic hard turned specimens. This is assumed to be caused by a combination of the higher hardness of the initial state of batch B, resulting from lower tempering temperature, as well as the different types of finishing processes. However, on basis of the presented results, this cannot be proofed finally and is objective of further investigations.

In summary, for both batches, only the cyclic plasticity is affected by the finishing processes, which cannot be explained with the microstructural details observed in SEM. Consequently, the different finishing processes seem to result in changes of the subsurface volumes on a smaller scale. As finishing processes generally lead to significant changes in the residual stress state,[15,16] the residual stresses within the subsurface volumes of the different conditions were analyzed, which is presented in Section 3.2.

3.2. Finishing-Induced Residual Stress State Within the Subsurface Volume

3.2.1. Batch A: Roller Bearing Rings

In **Figure 8**, the residual stresses in circumferential and axial direction within the subsurface volume are illustrated for the differently finished roller bearing rings. The regression lines shown in Figure 8 (and in **Figure 9**) are based on a B-spline interpolation between the single data points. Note that the regression lines are only a rough approximation of the real distribution of the residual stresses, which show slight deviations to the measured data points. Thereby, the deviations are more pronounced for the roller bearing rings, as smaller steps in electrolytic polishing, and thus, a higher spatial resolution, were used for the cryogenic hard turned fatigue specimens (compare Figure 8 and 9).

Comparing the residual stresses of the ground conditions, the fine ground bearing ring reveals in both directions significantly higher compressive residual stresses than the rough ground variant. However, for both conditions, only compressive residual stresses are measured at the surface and in the subsurface volume, which are maximum directly at the surface and are relieved nearly to 0 at a depth of $\approx 30\,\mu m$, respectively. Consequently, a more pronounced gradient in residual stresses beneath the surface is seen for the fine ground bearing rings.
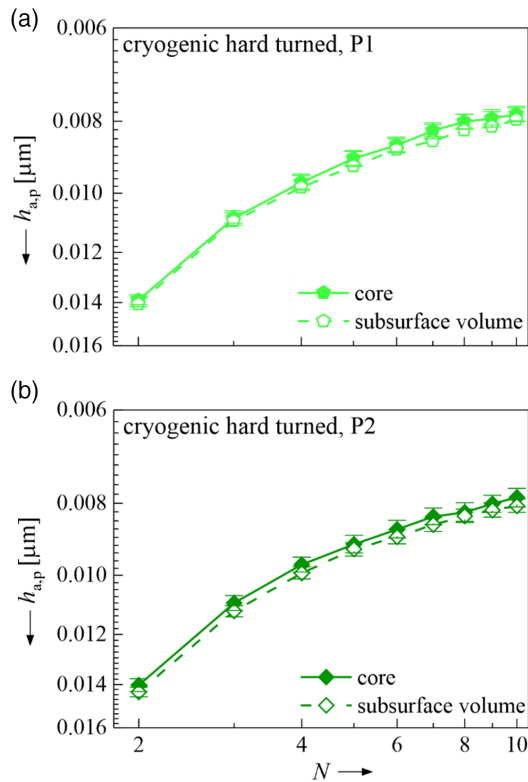
Figure 7. Comparison of the $h_{a,p}-N$ curves obtained in CITs within the subsurface volume and the core material of fatigue specimens cryogenic hard turned with different parameter sets a) P1 and b) P2.

In contrast to the ground roller bearing rings, the hard turned variant exhibits in circumferential direction tensile residual stresses directly at the surface, which turn to compressive residual stresses within the subsurface volume. Moreover, in axial direction, only small compressive residual stresses are observed directly at the surface after hard turning. For both directions, the maximum in compressive residual stresses is obtained for hard turned condition at a distance from the surface of $\approx 30\,\mu m$. As at this depth, the ground conditions show nearly no residual stresses, the compressive residual stresses are significantly more expanded in the hard turned condition. Furthermore, for the hard turned variant, the residual stresses are relieved nearly to 0 at a depth of roughly $75\,\mu m$.

Consequently, the residual stress measurements show a significant influence of the finishing process on the subsurface volume, which correlates with the differently pronounced increase in cyclic plasticity obtained in CITs.

3.2.2. Batch B: Fatigue Specimens

In correlation with the ground roller bearing rings, the cryogenic hard turned fatigue specimens exhibit in both directions compressive residual stresses at the surface and within the subsurface volume (see Figure 9). However, in contrast to the ground roller bearing rings, for P1 and P2, the maximum compressive residual stresses are observed in both directions at $\approx 20\,\mu m$ beneath the surface, respectively. This roughly correlates with the distributions of residual stresses of the hard turned roller bearing ring, whereby the cryogenic hard turned fatigue specimens show significantly higher values of compressive residual stresses (compare Figure 8 with 9).

Comparing the different parameter sets of cryogenic hard turning, P2 results in higher compressive residual stresses in both directions, which are slightly more expanded in relation to P1 condition (see Figure 9). While P1 results in a stress-free state at a depth of roughly $60\,\mu m$, the P2 condition reveals slight compressive residual stresses at this depth, which underlines the
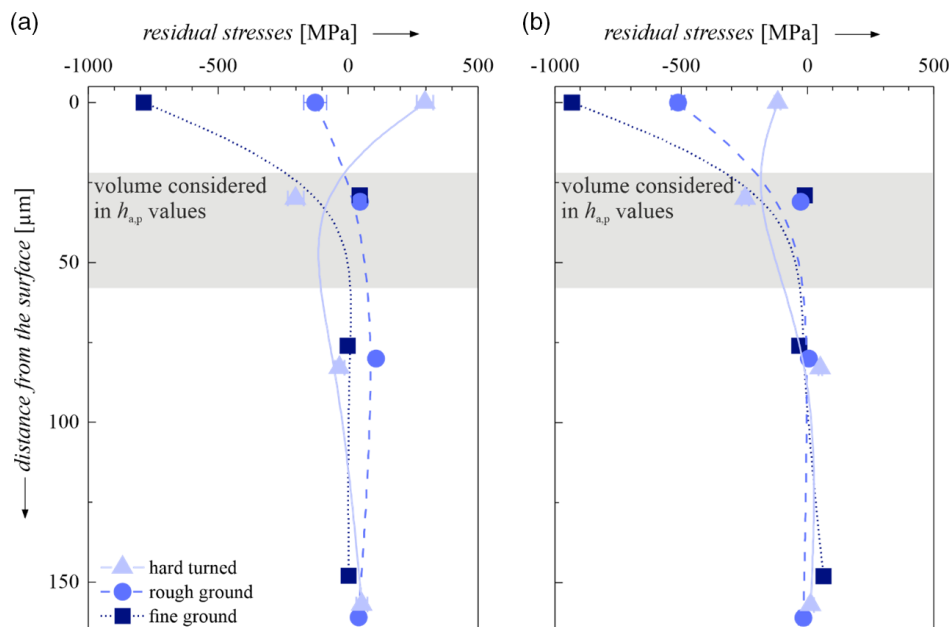

Figure 8. Residual stresses determined within the subsurface volumes of differently finished roller bearings in a) circumferential and b) axial direction.
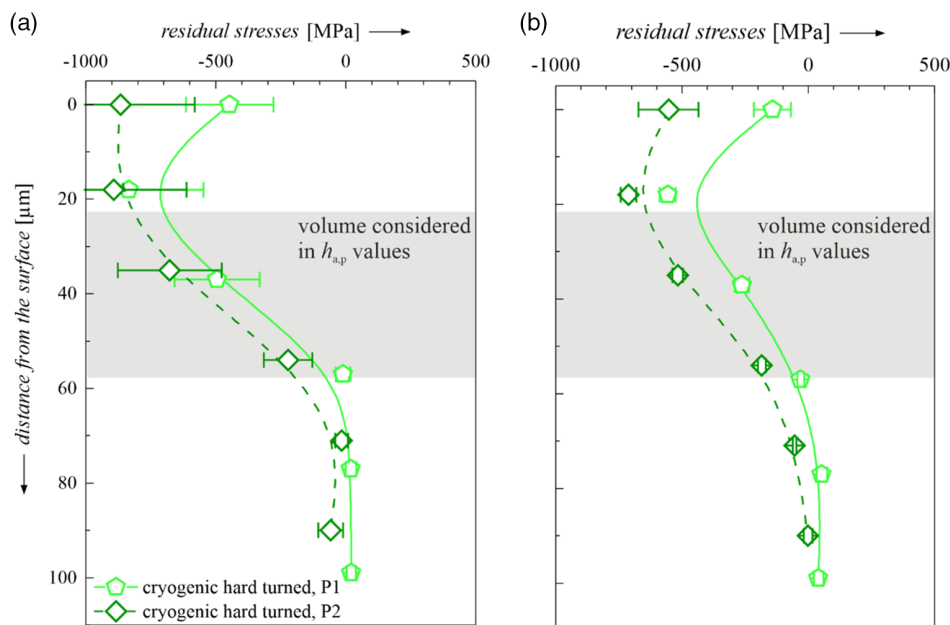
**ADVANCED
SCIENCE NEWS**

www.advancedsciencenews.com

**steel
research**
international

www.steel-research.de

Figure 9. Residual stresses determined within the subsurface volumes of differently cryogenic hard turned fatigue specimens in a) circumferential and b) axial direction.

bigger expansion of residual stresses for this condition. However, at a depth of $\approx 70\,\mu m$, also the fatigue specimen cryogenic hard turned with P2 exhibits nearly no residual stresses.

In summary, the different parameter sets of cryogenic hard turning result in slightly different residual stress states. This correlates with the differently pronounced increase in cyclic plasticity of the subsurface volume.

Note that the differences observed in CITs and XRD analyses on fatigue specimens of batch B are relatively small and are significantly less pronounced compared to the results obtained from batch A. However, for both batches, the different finishing processes result in differences in the distribution of the residual stresses as well as in the increase in cyclic plasticity of the subsurface volume. Consequently, the changes in $h_{a,p}-N$ curves and the residual stress states are compared for all conditions in Section 3.3.

3.3. Comparison of the Residual Stresses and the Cyclic Plasticity Obtained in CITs

Comparing the distribution of the residual stresses in the subsurface volume and the $h_{a,p}-N$ curves, it has to be considered that the plastically deformed zone beneath the indenter is expanded far beyond the indentation point, that is, roughly three times the indent diagonal.[20] Thus, the residual stresses measured at a defined distance from the surface are not one to one comparable with the results obtained in CITs. The $h_{a,p}-N$ curves are the result of an integration of the plastically deformed material volume beneath the indenter, which is illustrated schematically with the gray-shaded areas in Figure 8 and 9. Note that the stress distribution beneath the indenter is not homogenous, resulting in higher stresses and hence, more pronounced plastic

deformation in the direct vicinity of the indenter.[36] Consequently, the material volume in the direct vicinity of the indenter contributes more to the $h_{a,p}-N$ curves than the surrounding, less-deformed regions. Moreover, the residual stresses of both directions have to be considered, as the indentation results in a multiaxial stress state. Because of these complex interrelations, only a qualitative comparison of the cyclic plasticity observed in $h_{a,p}-N$ curves and the residual stress state is made in the following sections.

For this qualitative comparison, in **Figure 10**, the changes in cyclic plasticity between the subsurface volume and the core material are related with the respective residual stresses within the volume considered in CITs. To quantify the increase in cyclic plasticity of the subsurface volume, the $h_{a,p}$ value obtained in the tenth cycle in CITs was subtracted by the respective value determined for core material. This difference in cyclic plastic deformation is defined as $\Delta h_{a,p\,10}$, whereby higher values represent a more pronounced increase in cyclic plasticity of the subsurface volume. As a representative of the residual stresses, for both directions, the mean value of the residual stresses within the volume considered in CITs was determined based on the regression curves shown in Figure 8 and 9 (see Figure 10a). As the stress distribution beneath the indenter is inhomogeneous, this value only serves as a rough approximation of the residual stress state. As the different batches are not comparable with each other, this correlation between increase in cyclic plasticity and residual stress state is discussed separately for the different batches.

3.3.1. Batch A: Roller Bearing Rings

As shown in Figure 10b, the subsurface volumes show positive $\Delta h_{a,p\,10}$ and thus, an increased cyclic plasticity in relation to the
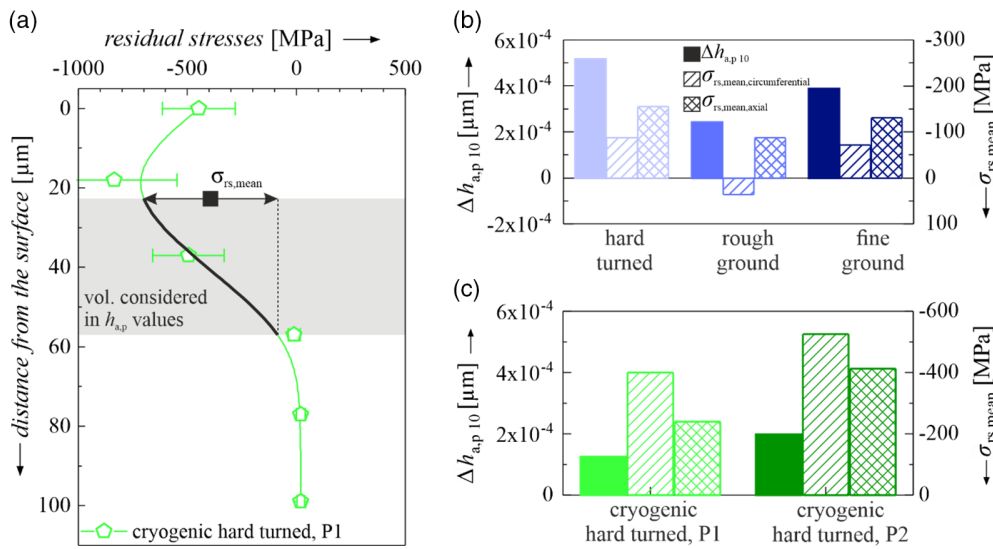
Figure 10. a) Schematic description of the determination of the mean value of the residual stresses on the example of the fatigue specimen cryogenic hard turned with P1 as well as the illustration of the relation of change in cyclic plasticity, represented by $\Delta h_{a,p\,10}$, and the mean value of residual stresses in axial and circumferential direction for b) differently finished roller bearing rings and c) cryogenic hard turned fatigue specimens.

core material volumes, which correlate with compressive residual stresses in the volume plastically deformed in CITs (gray shaded in Figure 8). As the indentation mostly leads to compressive stresses in the material, it is assumed that compressive residual stresses contribute to a more pronounced plastic deformation and thus, higher $h_{a,p}$. This further explains the most pronounced increase in cyclic plasticity observed for the subsurface volume of hard turned condition, which shows the highest level of compressive residual stresses at the considered distance from the surface (see Figure 10b). The rough ground condition shows small tensile stresses in circumferential direction. However, as the compressive residual stresses in axial direction are extensively bigger than these small tensile stresses, for this condition, compressive residual stresses are expected to be dominating within the subsurface volume, which correlates with a slight increase in cyclic plasticity.

Although the ground-bearing rings reveal higher maximum compressive residual stresses, these maxima are located directly at the surface and thus, have a smaller impact on the $h_{a,p}-N$ curves than the maximum compressive stresses measured for the hard turned condition at a distance from the surface of $\approx$30 μm. This is further underlined by the mean values of residual stresses within the relevant volume (see Figure 10b). However, also the compressive residual stresses measured for the ground conditions seem to influence the $h_{a,p}-N$ curves, as the subsurface volumes show higher values of $h_{a,p}$, resulting in positive values of $\Delta h_{a,p10}$ in Figure 10b. Furthermore, the fine ground condition shows a more pronounced increase in cyclic plasticity of the subsurface volume in relation to the rough ground roller bearing ring. This correlates with a higher level of the compressive residual stresses measured in both directions. This further corresponds to the assumption of higher $h_{a,p}$ due to compressive residual stresses.

3.3.2. Batch B: Fatigue Specimens

For both sets of parameters used for cryogenic hard turning, a higher cyclic plasticity as well as significant compressive residual stresses are observed in the volume plastically deformed during CITs (see Figure 10a,b), which supports the assumption that residual compressive stresses result in higher values of $h_{a,p}$. Furthermore, P2 reveals little higher compressive residual stresses, as well as a slightly more pronounced increase in cyclic plasticity in the subsurface volume, which also corresponds to this hypothesis.

This correlation between compressive residual stresses and increase in cyclic plasticity in $h_{a,p}-N$ curves is differently pronounced between batch A and batch B, whereby the effects on cyclic plasticity are more clearly for the roller bearing rings, which show lower compressive residual stresses in the relevant area (see Figure 10b,c). This might be caused by the higher strength of batch B, leading to smaller plastic deformation capability and thus, less pronounced effects on cyclic plasticity. Moreover, the results obtained in CITs are not only dependent on the residual stress state, but also on microstructural phenomena like, for example, dislocation density, as well as carbide size and distribution, which are related to the initial state of the material (e.g., heat treatment condition). However, for material conditions identical in the initial state, a correlation between an increased cyclic plasticity obtained from the $h_{a,p}-N$ curves and the residual stress state is shown in Figure 10b,c. Thus, the presented results indicate that the PhyBaL$_{CHT}$ method can be used for a rough estimation of the residual stress distribution induced by different finishing processes. Nevertheless, this has to be proofed in further investigations for other materials and material conditions, which is objective of future research work.

ADVANCED
SCIENCE NEWS

www.advancedsciencenews.com

steel
research
international

www.steel-research.de

4. Summary and Conclusion

In the present work, the influence of different finishing processes on the subsurface morphology of AISI 52100-bearing steel is determined, which comprises in the present work the surface and the volume beneath the surface up to a distance from the surface of ≈50−60 µm. Therefore, roller bearing rings were finished using hard turning, fine grinding, and rough grinding. In addition to these established finishing processes, fatigue specimens were cryogenic hard turned using two different sets of parameters. The finishing-induced residual stresses within the subsurface volume were determined by means of XRD measurements at different distances from the surface. Moreover, these results are compared with the cyclic deformation behavior obtained from instrumented CITs, as well as with microstructural investigations. From the presented results, the following conclusions can be drawn.

1) In scanning electron microscopy, no significant microstructural changes were observed in the subsurface volume compared with the respective core material volume.

2) The different finishing processes used for roller bearing rings result in significantly different residual stresses, whereby the fine ground condition shows the highest compressive residual stresses, which are located directly at the surface. In contrast to that, hard turning resulted in a maximum of the compressive residual stresses beneath the surface. Similar to the hard turned bearing ring, the cryogenic hard turned fatigue specimens also showed pronounced compressive residual stresses, being maximal beneath the surface.

3) Comparing the results obtained in CITs, the different finishing processes did not lead to changes of the cyclic hardening potential as well as hardness within the subsurface volume in relation to the respective core material, which correlates with scanning electron microscopy. However, for all conditions, a higher cyclic plasticity was obtained in the subsurface volume than in the core material. This is assumed to be caused by the compressive residual stresses resulting from finishing processes.

The correlation of cyclic plasticity obtained in CITs and compressive residual stresses measured by XRD indicates that cyclic indentation testing has the potential to enable a rough estimation of the distribution of the residual stresses of a material, if there are no significant gradients in microstructure and associated local hardness. Nevertheless, this has to be confirmed by further experiments at other materials and material conditions, which is objective of future research.

Conflict of Interest

The authors declare no conflict of interest.

Data Availability Statement

Research data are not shared.

[1] D. Frölich, B. Magyar, B. Sauer, P. Mayer, B. Kirsch, J. C. Aurich, R. Skorupski, M. Smaga, T. Beck, D. Eifler, *Wear* **2015**, 328–329, 123.

[2] B. B. Bartha, J. Zawadzki, S. Chandrasekar, T. N. Farris, *Metall. Mater. Trans. A* **2005**, 36, 1417.

[3] M. Smaga, R. Skorupski, D. Eifler, T. Beck, *J. Mater. Res.* **2017**, 32, 4452.

[4] S. Smith, S. N. Melkote, E. Lara-Curzio, T. R. Watkins, L. Allard, L. Riester, *Mater. Sci. Eng. A* **2007**, 459, 337.

[5] S. B. Hosseini, K. Ryttberg, J. Kaminski, U. Klement, *Proc. CIRP* **2012**, 1, 494.

[6] T. Neubauer, in *Betriebs- Und Lebensdauerverhalten Hartgedrehter Und Festgewalzter Zylinderrollenlager, PhD Thesis*, Gottfried Wilhelm Leibniz Universität Hannover, Hannover **2016**.

[7] P. J. Romanowicz, B. Szybiński, *Materials* **2019**, 12, 4194.

[8] J. Kalisz, D. Toboła, *Mechanik* **2019**, 92, 718.

[9] T. Fujita, N. Hasegawa, N. Kamura, T. Sasaki, *Tribol. Online* **2019**, 14, 163.

[10] S. Basten, B. Kirsch, W. Ankener, M. Smaga, T. Beck, J. Uebel, J. Seewig, J. C. Aurich, *Proc. CIRP* **2020**, 87, 77.

[11] W. Ankener, J. Uebel, S. Basten, M. Smaga, B. Kirsch, J. Seewig, J. C. Aurich, T. Beck, *Proc. CIRP* **2020**, 87, 119.

[12] R. Bertolini, V. Bedekar, A. Ghiotti, E. Savio, R. Shivpuri, S. Bruschi, *Int. J. Adv. Manuf. Technol.* **2020**, 108, 1983.

[13] M. Biček, F. Dumont, C. Courbon, F. Pušavec, J. Rech, J. Kopač, *J. Mater. Process. Technol.* **2012**, 212, 2609.

[14] D. Umbrello, *Int. J. Adv. Manuf. Technol.* **2013**, 64, 633.

[15] B. Denkena, T. Grove, O. Maiss, *Proc. CIRP* **2016**, 45, 359.

[16] M. Jacobson, F. Gunnberg, *Proc. Inst. Mech. Eng. B J. Eng. Manufact.* **2004**, 218, 457.

[17] B. Denkena, G. Poll, O. Maiß, T. Neubauer, *AMR* **2014**, 966–967, 425.

[18] F. Sadeghi, B. Jalalahmadi, T. S. Slack, N. Raje, N. K. Arakere, *J. Tribol.* **2009**, 131.

[19] P. Romanowicz, B. Szybiński, *AMM* **2014**, 621, 95.

[20] P. Sadrabadi, K. Durst, M. Göken, *Acta Mater.* **2009**, 57, 1281.

[21] K. Durst, B. Backes, M. Göken, *Scr. Mater.* **2005**, 52, 1093.

[22] H. S. Kramer, P. Starke, M. Klein, D. Eifler, *Int. J. Fatigue* **2014**, 63, 78.

[23] B. Blinn, D. Görzen, M. Klein, D. Eifler, T. Beck, *Int. J. Fatigue* **2019**, 119, 78.

[24] T. Saraswati, T. Sritharan, S. Mhaisalkar, C. D. Breach, F. Wulff, *Mater. Sci. Eng. A* **2006**, 423, 14.

[25] H. M. Sajjad, H. Ul Hassan, M. Kuntz, B. J. Schäfer, P. Sonnweber-Ribic, A. Hartmaier, *Materials* **2020**, 13, 3126.

[26] M. W. Klein, B. Blinn, M. Smaga, T. Beck, *Int. J. Fatigue* **2020**, *134*, 105499.

[27] B. Blinn, D. Görzen, T. Fischer, B. Kuhn, T. Beck, *Appl. Sci.* **2020**, *10*, 6461.

[28] S. Deldar, I. Alabd Alhafez, M. Smaga, T. Beck, H. M. Urbassek, *Metals* **2019**, *9*, 541.

[29] D. Görzen, H. Schwich, B. Blinn, W. Song, U. Krupp, W. Bleck, T. Beck, *Int. J. Fatigue* **2021**, *144*, 106042.

[30] B. Blinn, F. Krebs, M. Ley, R. Teutsch, T. Beck, *Int. J. Fatigue* **2020**, *131*, 105301.

[31] Z. Zurecki, R. Ghosh, J. H. Frey, in *Proc. of IMECE'03*, Air Products and Chemicals, Inc., Washington, D.C. **2003**, pp. 211–220.

[32] D. J. Hornbach, P. S. Prevéy, P. W. Mason, in *First Int. Conf. on Induction Hardened Gears and Critical Components*, Gear Research Institute, Indianapolis, IN **1995**, pp. 69–76.

[33] J. Holmberg, A. Steuwer, A. Stormvinter, H. Kristoffersen, M. Haakanen, J. Berglund, *Mater. Sci. Eng. A* **2016**, *667*, 199.

[34] DIN-Normenausschuss Materialprüfung, in *Metallische Werkstoffe – Instrumentierte Eindringprüfung Zur Bestimmung Der Härte Und Anderer Werkstoffparameter – Teil 1: Prüfverfahren*, Beuth Verlag GmbH, Berlin **2015**.

[35] P. S. Prevéy, in *Metals Handbook*, Vol. *10* (Ed: R.E. Whan), American Society for Metals, Metals Park, OH **1986**, pp. 380– 392.

[36] G. Feng, S. Qu, Y. Huang, W. D. Nix, *Acta Mater.* **2007**, *55*, 2929.

2100253 (11 of 11)